Performance of a three-ton liquid argon time projection chamber

P. Cennini, S. Cittolin, J-P. Revol, C. Rubbia, W-H. Tian

CERN, CH-1211, Geneva 23, Switzerland

P. Picchi

Lab. Naz. di Frascati dell'INFN, via E. Fermi 40, Frascati, Roma, Italy

F. Cavanna, G. Piano Mortari, M. Verdecchia

Dipartimento di Fisica e INFN, Università dell'Aquila, via Vetoio, Coppito (AQ), Italy

D. Cline, G. Muratori, S. Otwinowski, H. Wang, M. Zhou

Department of Physics, UCLA, Los Angeles, CA 90024, USA

A. Bettini *, F. Casagrande, P. Casoli, S. Centro, B. Dainese, C. De Vecchi, A. Pepato, F. Pietropaolo, P. Rossi, S. Ventura

Dipartimento di Fisica e INFN, Università di Padova, via Marzolo 8, Padova, Italy

P. Benetti, E. Calligarich, R. Dolfini, A. Gigli Berzolari, F. Mauri, L. Mazzone, C. Montanari, A. Piazzoli, A. Rappoldi, G.L. Raselli, D. Scannicchio

Dipartimento di Fisica e INFN, Università di Pavia, via Bassi 6, Pavia, Italy

L. Periale, S. Suzuki

ICGF del CNR di Torino, corso Fiume 4, Torino, Italy

We have constructed and operated a 3 ton liquid argon time projection chamber as part of the R&D programme for the ICARUS project. We report on the analysis of events from cosmic rays and from radioactive sources collected from June 1991 to June 1993. We have systematically investigated the performance and the physical parameters of the detector. We present here the results obtained from the analysis of the cosmic rays data on the following items: the electron drift velocity, the electron lifetime, the free electron yield, the electron diffusion coefficient, the space resolution and the particle identification capability. The data from radioactive sources are used to study the energy resolution in the MeV range. The in depth understanding of the basic physics aspects of the liquid argon TPC allows us to conclude that such a detector can be built in large sizes and reliably operated over long periods of the time, providing a new instrument for physics experiments.

1. Introduction

The ICARUS collaboration proposed [1] in 1985 a multi-kiloton LAr TPC to be operated in the Gran Sasso Laboratory to search for rare underground phenomena ranging from proton decay to real time solar neutrino observations, as well as neutrino oscillations and relic supernovae neutrinos.

As a part of our research and development programme we built a medium scale prototype, with a mass of 3 tons. Beginning on June 1991 we started to collect data to measure the relevant physical parameters of the detector, to understand its response to ionising events in a wide energy range from the MeV to the GeV scales and to gain operating experience on a long time. The results reported here are based on the cosmic ray data collected from June 1991 to the end of December 1992.

* Corresponding author.

We have described the construction of the 3 ton detector in a separate paper, where we have also shown some bubble chamber grade event images [2]. Physics results based on the analysis of the data will be discussed in the present paper. We have measured the parameters that determine the behaviour of the detector: electron lifetime, electron drift velocity, free electron yield, electron diffusion coefficient, space resolution and particle identification capability. We have also taken data from radioactive sources to study the energy resolution.

2. The three-ton detector

We have fully described the three-ton prototype detector, its construction and operation in ref. [2], and simply recall here its principal characteristics. The inner volume (2.61 m^3) is split into two independent semicylindrical sections. Both sections are equipped with identical drift chamber systems. Each wire chamber covers a surface equal to 2.4×0.9 m^2 and is supported by frames. The drift volume is defined by the chamber itself, a system of "race tracks", used to produce a uniform electric field in the drift region. The maximum drift distance is 42 cm. The monitor chambers we use for measuring and controlling the electron lifetime have been described elsewhere [3]. We only mention here that the monitor is a doubly gridded ionisation chamber; the maximum measurable lifetime is between 2 and 3 ms. A monitor chamber is located at the bottom of the detector and is used to monitor continuously the electron lifetime. With one exception that we will now describe, during the more than two years long operation it has always been found to be between 2 and 3 ms. These values have been checked, always finding consistent results, by measuring (see section 7) the charge deposited on the wires by vertical cosmic ray muons and observing the shift of the distribution peak position for increasing distances of the track from the collecting wires.

The ultra pure liquid argon, even in the absence of any leak, can be contaminated by outgassing of the walls and of the various materials (electrodes, chambers, spacers, cables, high-voltage resistors, etc.) contained in the dewar. In practice the main outgassing sources are the parts of the system that are not in direct contact with the liquid and have as a consequence higher temperatures. The closing flange and the signal cables in particular have large surfaces in the clean volume at almost room temperature and are the main source of outgassing. To keep the liquid argon at the necessary purity we have provided a recirculation system. The naturally evaporating argon is brought through a pipe to a purification system similar to the main one. The argon is then recondensed in a serpen-

tine. The hydraulic circuit just described is ultra-clean. The system provides a natural compensation of the thermal losses of the detector dewar. As we will show, the recirculation system, described in ref. [2], proved to be an essential part of the apparatus necessary to maintain the purity of the argon.

This conclusion has been strengthened by the incident and the subsequent recovery that we will now describe.

During the night of December 31, 1992 a power-off caused the stop of the pumping system that keeps the vacuum in the insulation space between the internal and the external vessels of the dewar. The fault was detected only after a few hours; during this time excess heat flowed into the liquid. When we measured the electron lifetime after the accident we found it to be 150 μs. Searching for leaks, we found that the rupture disk (a 100 μm thick stainless steel membrane used for safety reasons) had a small crack.

Tests on ultra pure liquid argon, in separate containers, had shown that the contamination of the liquid by oxygen present in the gas above its free surface is extremely slow, provided there are no convective motions in the liquid. It is on the other hand practically immediate in the presence of motions in the liquid [3]. This behaviour is due to the slowness of the diffusion from gas into the liquid. It is of great importance for a reliable operation of the detector. We then interpreted the lifetime degradation as due to the insurgence of convective motions in the ultrapure liquid during the excess heat input period. These motions have mixed the liquid with the gas above it that was contaminated with oxygen.

The proof that our interpretation is likely to be correct is given by the fact that, after having repaired the rupture disk, the measured values of the lifetime started to increase exponentially in time at the rate expected from the known evaporation rate. This demostrates clearly the power of the recirculation system. We display in Fig. 1 the electron lifetime, as measured with crossing muons tracks, as a function of time (the values measured by the monitor chamber are compatible). During the exponential rise the slope corresponds to an evaporation rate of 3.2 l/h. Subsequently the lifetime reached, and even exceeded, the value it had before the accident.

We can conclude that, even in the presence of an exceptional event that causes contamination of the liquid, a suitably designed recirculation system can lead to a quick recovery of the operational conditions.

3. The readout

The readout is performed with a chamber consisting of three parallel wire planes located at the end of the
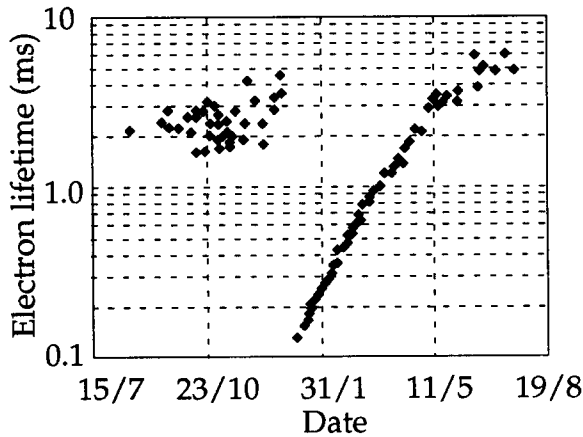
Fig. 1. Electron lifetime from 15/7/92 to 19/8/93 as measured using crossing tracks.

Fig. 2. Charge collected by the induction wires as a function of field ratio across the grid.

drift length. We call z the coordinate along the electric field, x and y the coordinates on the plane of the chamber. The absolute z coordinate is given by a measurement of the drift time, provided that $t = 0$ time and drift speed are known. The drifting electrons reach and cross in sequence the following wire planes: 1) a plane of wires running in the y direction, functioning as the screening grid; 2) a plane of wires (2 mm pitch) running again in the y direction, located at a distance of 2 mm below the screening grid where its function is to measure by induction the x coordinate (we call it "induction plane" in the following); 3) a plane of wires running in the x direction, with 2 mm pitch, located at a distance of 2 mm below the induction plane; its function is to measure the y coordinate. Since this is the last sensitive plane the electric field is arranged to collect the drifting electrons (collection plane).

The ratio of the electric fields above the screening grid (E_1) and between it and the induction plane (E_2) is chosen to achieve full transparency of the grid. Fig. 2 shows the average charge produced by a minimum ionising track and collected by the single sense wires as a function of $E_2 : E_1$. As predicted by the Buneman's formula [4], full transparency is reached at $E_2 : E_1 = 1.4$. We will discuss the data collected at $E_2 : E_1 = 1.5$.

The collection plane is made of sense wires at a 2 mm pitch separated by screen wires. The fields above (E_2) and below the induction plane (E_3) are chosen to assure complete transparency of the induction plane. Fig. 3 shows the average charge collected by the single sense wires produced by a minimum ionising track as a function of $E_3 : E_2$. As predicted, full transparency is reached at $E_3 : E_2 = 3.1$. The data to be discussed here have been collected at $E_3 : E_2 = 3.5$.

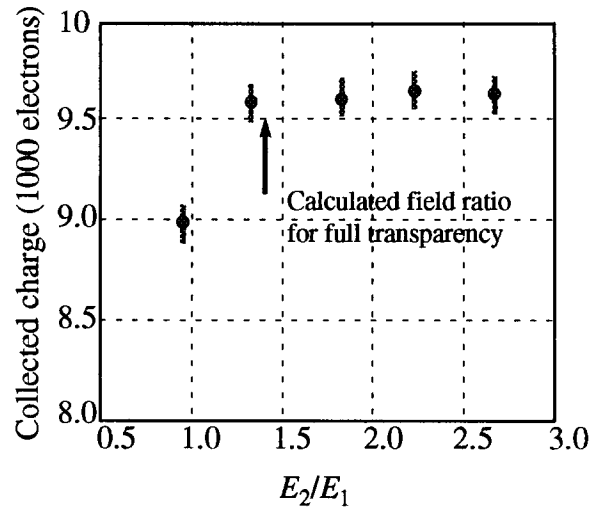The current signals from each sense wire of the induction plane and of the collection plane are inte-

grated by charge sensitive preamplifiers. The preamplifiers are located close to the signal feedthroughs to minimise the input capacitance and hence the noise.

For a minimum ionising track parallel to the chamber the shape of the charge signal from the induction plane is triangular with a maximum of about 6000 electrons for a 2 mm sample (depending on the field intensity). Fig. 4 shows an example of a digitised induction signal, where two tracks are present, sampled with a 200 ns period. As expected from our calculations, the induced charge is not the full charge crossing the wire plane, but only 60% of it.

The charge signal from the collection plane is a step function followed by the exponential discharge of the capacitor that holds the charge. The height of the step
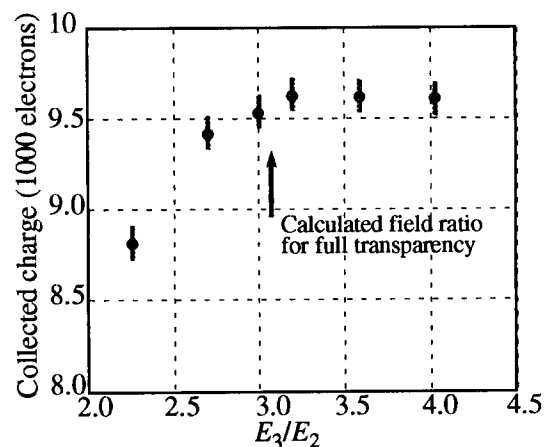

Fig. 3. Charge collected by the induction wires as a function of field ratio across the induction plane.
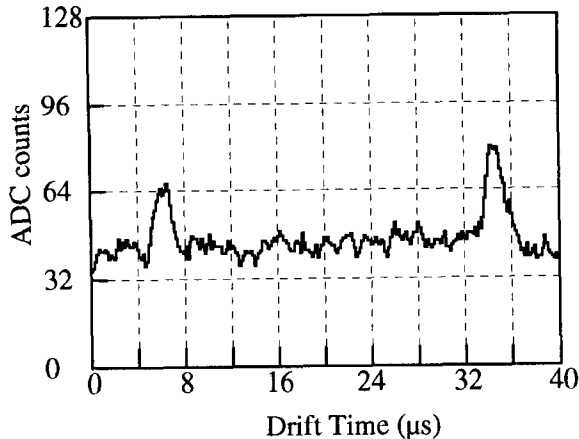
Fig. 4. A digitised induction signal on one doublet, showing the presence of two tracks. Sampling period is 200 ns

is around 10 000 electrons for a 2 mm sample. Fig. 5 shows an example of a digitised collection signal, sampled with a 200 ns period, together with the curve resulting from the filtering and fitting procedure we will describe. Two close tracks contribute to the signal: their distance in time is 4.6 μs (from fit). The drift velocity is 1.24 mm μs: the distance between the two tracks along the drift direction is then 5.7 mm. It is clear from the example that the two track resolution is close to the 2 mm length of the gaps between the wire
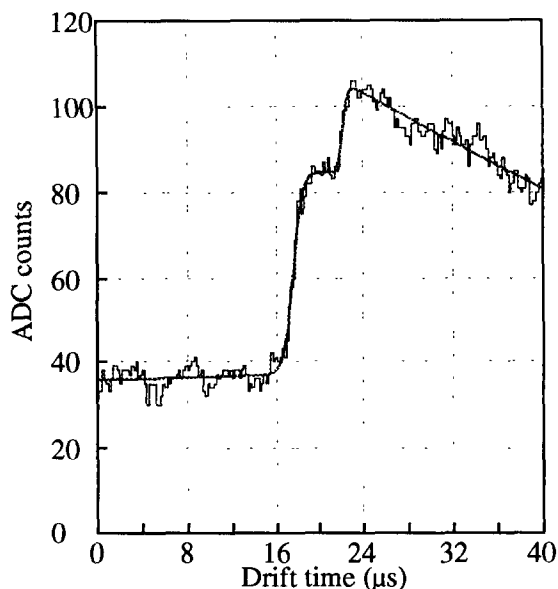

Fig. 5. A digitised signal from one collected wire due to two tracks separated by 5.7 mm. The curve is the result of the fitting procedure described in the text.

planes. The value of the rise time obtained from fit is 2.4 μs.

We notice that the signal may become very long, several microseconds, if the track has a large dip angle. This requires that the low frequency components must be accepted by the amplifier without distortion.

The capacitance at the input of the amplifiers is the sum of the wire and of the cable capacitances, the latter being the larger. The input capacitance range from 100 pF for the upper collection wires to 200 pF for the induction wires. The corresponding design equivalent noise charge (ENC) evaluated with 1 μs shaping time is ENC (electrons) = $500 + 2.5C$, where C is the input capacitance in pF, corresponding to values between 700 and 1000 electrons. These values have been confirmed by direct measurements on the detector.

The charge signals are sampled with flash ADCs (one per channel) at a frequency that provides several measurements for each pulse. The sampling period ranges from 50 to 400 ns; we have used 200 ns period in the data collection described in this work. The complete readout system is described in ref. [2]. The charge measurement calibration is obtained for all channels by injecting the same voltage pulse on test capacitances (one per channel). The test capacitances have been measured with 0.5% accuracy. The gains have been periodically measured and found to be stable within 2%.

Two different types of cross talk are present between electronic channels. The first one is the cross talk between two contiguous wires: its average value is 1.2%. The second one is due to the structure of our cables. The signals from groups of eight contiguous wires are brought from the chamber to the amplifiers by specially designed flat cables. A number (32) of these flat cables are sandwiched together to form a stack as described in ref. [2]. The cross talk between a wire in one cable and the octet that it faces is on average 1%.

4. Extraction of the signal

As mentioned above the charge signals are small and the signal-to-noise ratios are S/N ≈ 10 for the collection wires and S/N ≈ 6 for the induction doublets. We are discussing here the software filtering algorithms and procedures developed to extract the relevant parameters (pulse time, rise time, height, etc.) from the digitised data.

The data used in this paper were obtained mainly from cosmic ray muons crossing almost vertically the detector: the information comes, as a consequence, mainly from the horizontal collection wires. We will describe the algorithms used to extract, from the digi-
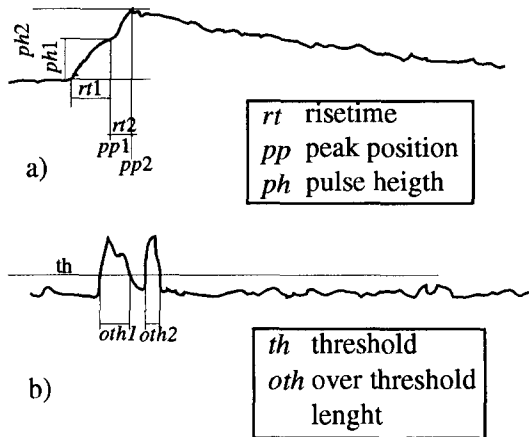
Fig. 6. (a) shows a sketch of the signal of Fig. 5, with the filter parameters symbols. (b) shows the filtered signal.

tised collection signals, the relevant information and its evaluation based on a sample of simulated vertical tracks.

The collection signal carries three main characteristics (Fig. 6a) which are relevant for the physics analysis: peak time position (pp), which gives the drift coordinate; pulse height (ph), proportional to the collected charge; rise time (rt), which depends both on the track angle with the plane, and on the diffusion of the electron cloud during the drift. These parameters are extracted in two steps: first, the valid regions (those which contain some signal over the noise) inside the large event data must be traced and a hit table is built; then, a least-squares fit is performed locally on each single region traced on the table, to recover the signal behaviour. The search region must be wide enough to accept inclined track signals and multiple hits from close tracks: we take a range of ± 50 samples around the peak. Searching in a long (20 μs) window corresponds to accept the low frequency part of the spectrum, where $1/f$ and microphonic noises give important contributions (larger than the signal itself). The hit finding algorithm must then be robust against noise

and it must perform with an efficiency close to 100% on the entire range of collection signals.

4.1. The hit finder

To find the hits we have chosen a two stage nonlinear filtering procedure. A nonrecursive median filter (5 samples long) is first applied to reduce high frequency disturbances contribution (electromagnetic pickup from surrounding devices, spikes due to FADC output swing on most significant bits). Then the local variance is calculated over a narrow window that spans the entire signal. The output (Fig. 6b) is a flat baseline around the noise level, with a peak quickly rising up as the collection rising edge enters the window. Given its small slope, the long (many window sizes) falling tail gives a negligible contribution to the variance, and the output lowers back just above the noise level. This allows for a clear separation of overlapping tracks. When the variance output stays over a given threshold (th) long enough (oth), that region is tagged as r.o.i. (region of interest) and passed to the fitting algorithm.

A Monte Carlo simulation has been developed to study the filter performance concerning signal and noise characteristics and to optimise the choice of the relevant filter parameters: window size, threshold level, over-threshold width).

Fig. 7 shows the efficiency of the hit finding algorithm, for two different noise levels, as a function of the threshold parameter. Units are ADC counts, one ADC count corresponding to 350 electrons. A white noise is included in the Monte Carlo simulation. Its rms value is 3 ADC counts in Fig. 7a, 4.5 ADC counts in Fig. 7b. As mentioned in section 2 the ENC measured at 1 μs shaping time is typically 1000 electrons corresponding to 3 ADC counts. From the figures we see that, in both cases, the efficiency is close to 100% in a wide range of the parameter. We fix the threshold parameter at four times the noise level (i.e. at 12 ADC counts in Fig. 7a, and at 18 in Fig. 7b).

We then consider the hit finder efficiency (Fig. 8) (the rms noise is 3 ADC counts) changing the window width parameter. Again the efficiency is close to 100%
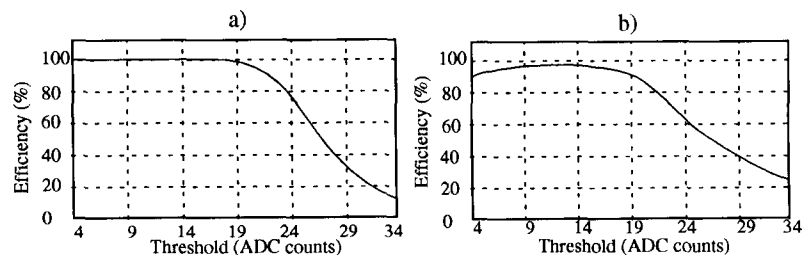

Fig. 7. Efficiency of the hit finding algorithm as a function of the threshold parameter. The rms noise is different in the two figures: 3 ADC counts in (a), 4.5 ADC counts in (b). 1 ADC count = 350 electrons.
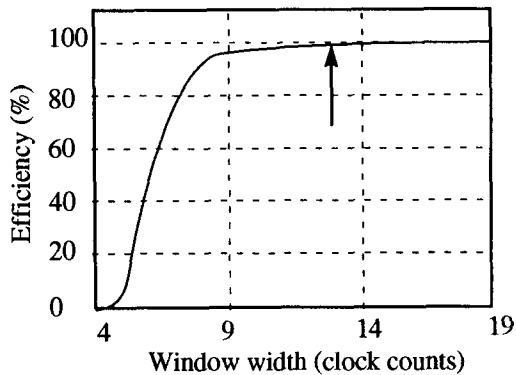
Fig. 8. Efficiency of the hit finding algorithm as a function of the window width. The threshold is four times the noise rms, the noise rms is 3 ADC counts. 1 clock count is 200 ns.

in a wide range and, as expected, the parameter must be chosen close to the rise time value, typically between 1.2 μs (6 clock counts) and 1.6 μs (8 clock counts). We fix the window width parameter at 13 clock counts (arrow in Fig. 8).

Having fixed the threshold and the window width, we now study the hit finder efficiency as a function of the width over threshold in Fig. 9 (the rms noise is 3 ADC counts). Again the efficiency is close to 100% over a wide range. The value we chose for this parameter is 7 clock counts (arrow in Fig. 9).

In conclusion the efficiency of the hit finder appears to be high (> 98%) and stable around the chosen values of the parameters, which, as a consequence, are not critical. We then can have confidence in our algorithm for the analysis of cosmic ray muons. Some adjustment of the parameters might nonetheless be necessary for tracks at vastly different angles.
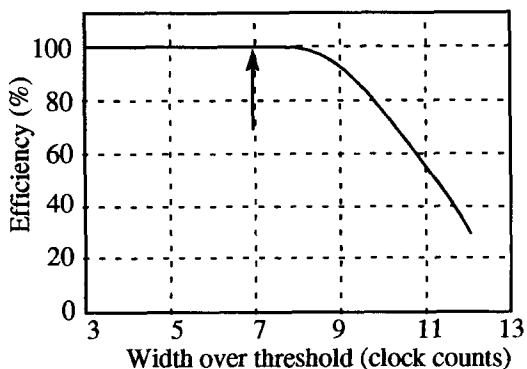

Fig. 9. Efficiency of the hit finder vs width over threshold. Noise rms = 3 ADC counts, threshold = 4 noise rms, window width = 12 clock counts. 1 clock counts = 200 ns, 1 ADC count = 350 electrons.

4.2. Fitting procedures.

The best way of extracting the physical quantities from the raw data in the r.o.i. is to perform a least-square fit to the data with a set of theoretical functions numerically computed by means of a simulation that incorporates the electron trajectories in liquid Ar, the signal they induce on the sense wires and the electronic response function. In practice, to speed up the calculation we use an analytical shape that reproduces well a wide range of signal shapes by means of few parameters (see Fig. 6): pulse height (ph), position in time (pp), rise time (rt), amplifier decay time (a) and includes a linear baseline $(a + bt)$. The function of the time t we use in the fit is (the decay time is fixed by direct measurement with the test pulse)

$$S(t) = \frac{phe(pp - t)/d}{1 + e(pp - t/rt)} + a + bt.$$

In the least square fitting procedure we chose an error on the single point equal to the rms noise used in the simulation. The minimum χ^2 is always close to the expected value, showing that the assumed analytical shape reproduces the signal correctly.

5. Electronic noise

The effective noise after off-line filtering and fitting is relative to a large bandwidth determined by the length of the search window and by the response function of the amplifier; its value may then be different from that, mentioned in section 2, measured with 1 μs shaping time. To measure it, we inject a series of test pulses of a fixed amplitude and a fixed rise time (similar to those of the track signals) in all the channels. The digitised outputs are then fitted with exactly the same procedures we used for the track signals, described in section 4. The distribution of the pulse heights, obtained by the fit, is shown in Fig. 10 for a test pulse height of 12 000 electrons. The curve is a Gaussian fit to data: the fitted value of the rms is 1300 ± 100 electrons. Notice also that any difference in the effective $t = 0$ amongst the channels due to different lengths of cables or different rise times is included in the rms value. We will see in section 10 that this is a small contribution.

The shape and the height of the charge signals from the tracks depend on the energy and angle of the track, on its distance from the wire plane and on the value of the electric field (due to recombination). The height of the charge signal depends on the energy deposited in a segment of track, whose length projected on the wire plane in the direction normal to the wires is equal to the pitch (2 mm). It also depends on the electric field, due to the recombination process (section 8) and, fi-
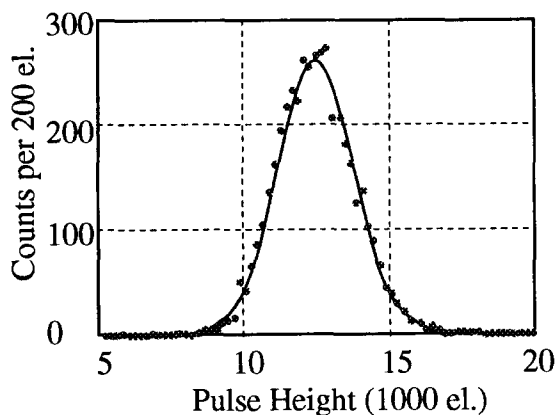
Fig. 10. Distribution of the measured charged for a test pulses of 12000 electrons. The width measures the electronic noise.

nally, on the drift time for finite values of the electron lifetime. For a constant value of the rms noise the S/N ratio and the resolution in the drift time measurement are correlated. The resolution in the drift time measurement is also a function of the signal rise time: for a given S/N ratio the resolution is of course smaller for shorter rise times. The rise time of the charge signal from the track elements depends mainly on two effects: a) the time taken by a point charge to cross the distance between the screening electrode and the sense wire plane. (With our geometry and field intensities this time varies between 1 and 2 μs); b) the time taken by the actual electron cloud to cross a given point; this is proportional to the diameter of the cloud and is an increasing function of the distance of the track from the wire plane, due to the diffusion process (section 8). Notice that the effect of diffusion is more important for a liquid TPC than for a gas TPC, where, due to the
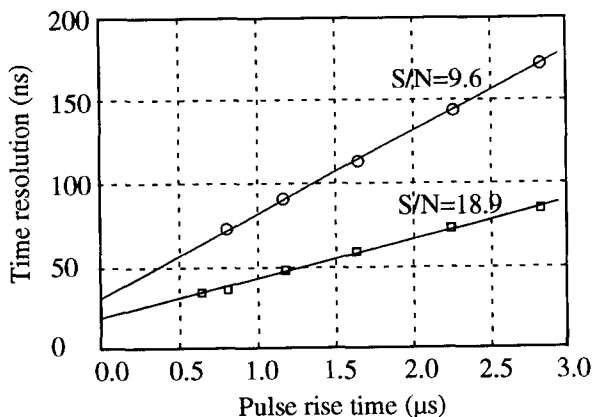

Fig. 11. Resolution on the time measurement as measured for test pulses of different rise times and of different amplitudes (different signal to noise ratios).
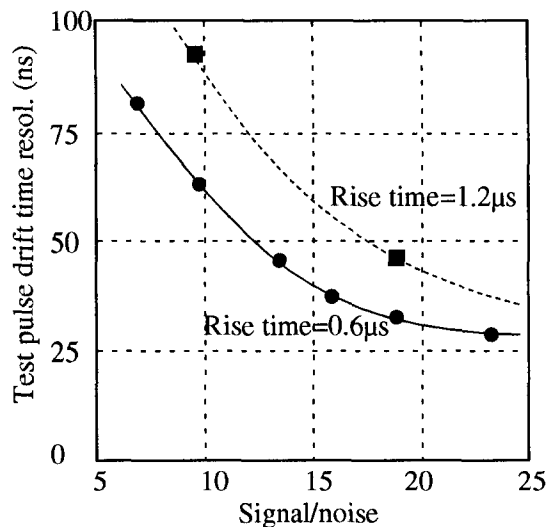

Fig 12. Contribution of the electronic noise to the resolution of the drift time measurement for two different values of the test pulse rise time. Curves are meant to guide the eye

amplification process, the resolution depends only on the fluctuations in the diffusion.

We use test pulse data to study the dependence of the time measurement on S/N and on rise time, by varying its amplitude and its rise time. For a series of test pulses of the same characteristics we define the resolution as the rms of a Gaussian fit to the measured time distribution.

Fig. 11 shows the measured time resolution as a function of the rise time for two different values of the S/N ratio. As it can be seen, the resolution is a linear function of the pulse rise time. Fig. 12 shows the time resolution as a function of the S/N ratio for two different rise times: a very fast one (0.6 μs) and one typical of our measurements (1.2 μs). In section 10 we will discuss the drift coordinate resolution for tracks and we will come back to these points.

6. Monte Carlo simulation

To have complete understanding of the physical processes that determine the behaviour of the detector we have developed a Monte Carlo simulation program, based on the GEANT Monte Carlo [5], that fully reproduces the detector response to all ionising events.

The simulation is performed in four steps:

a) In the GEANT framework the geometry of the detector (dewar, wire chambers, race track) is described as well as the characteristics of the materials used to build the detector (mainly steel and liquid Ar) and the definition of the active media (i.e.: the liquid Ar volume seen by the wire chamber).

b) Each particle initially defined by the user (particle type, energy, momentum and position) is propagated inside the detector by GEANT returning at each step the identity of the current particle, its energy, position and direction, the length of the last step, the amount of energy deposited and the mechanism of energy loss. The steps are performed until the particle exits the detector or looses its identity (i.e.: when it decays or its energy falls below the cut).

c) When a particle reaches the active medium, the energy deposited by ionisation is converted into charge (electrons) by means of the following formula (so-called Birks law):

$$dQ = \alpha \, dE / 1 + \beta \frac{dE}{dx},$$

which takes into account the increase of recombination probability with ionisation density. The parameters α and β have been chosen to reproduce the data obtained with stopping muon tracks in our detector (see section 8). The charge is then propagated in the liquid Ar taking into account the drift velocity given by the applied electric field and the diffusion coefficient. When each amount of charge reaches the wire chamber its value is stored into two bidimensional arrays, whose indexes are respectively the collection/induction hit wire number and the drift time (binned as in the real data).

d) When b) and c) have been completed, the stream of data corresponding to each wire is convoluted with a step function having finite rise time (typically ≈ 1 μs) to simulate the drift of the electrons between two successive wire planes. An equivalent noise charge is added to each time bin. The noise spectrum is assumed to be white for simplicity and its rms value is chosen to reproduce, in the output, the value (1300 electrons) measured with the test pulse as discussed in section 4. The result is then convoluted with the response function of the electronic chain (a double exponential with rise time ≈ 0.3 μs and decay time ≈ 42 μs) and is quantised in 256 levels following the ADC range used in the experiment (≈ 350 e/count).

Each event simulated in the way described above is then analysed using the same algorithms as for the data: the physical quantities extracted are then directly comparable with those obtained with analysis of the 3 ton detector data.

7. Drift velocity measurements

We have measured the electrons drift velocity as a function of the drift field using the purity monitor chamber outside the main dewar. The vapour pressure in the chamber was 1 bar, corresponding to a temperature of 87 K. The charge pulse length from the inte-
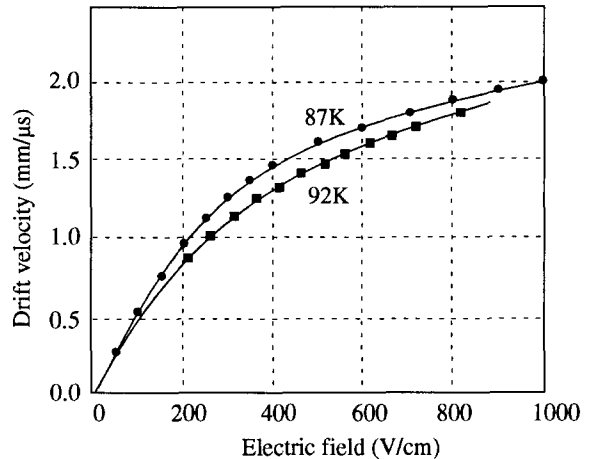

Fig. 13. Free electrons drift velocity in liquid argon as a function of the electric field. Circles at 87 K, squares at 92 K. Curves are to guide the eye

grating amplifier is equal to the drift time between the cathode and anode grids. For a given field the drift velocity is obtained dividing the grid distance (50 mm), by the measured drift time. Results are reported in Fig. 13.

An independent measurement was performed in the detector using muon tracks crossing diagonally the drift volume. The distance from the entrance point through the cathode (the first point of the track) and the point where the track crosses the collection plane (recognised as the point where the track image reflects) is known. The drift time is measured and recorded by the readout electronics. The vapour pressure was 1.5 bar corresponding to $T = 92$ K. Results are reported in Fig. 13. Data show a strong dependence of the drift velocity on temperature, implying that an accurate control of the vapour pressure is requested to have a reliable operation of the detector.

At low field values the drift velocity is approximately a linear function of the field, i.e. the mobility is a constant. When the drift velocity reaches values close to the sound speed (0.85 mm/μs) it increases less rapidly, approximately as $\sqrt{E}$. Mobility in the linear zone is 545 cm^2 V^{-1} s^{-1} at 87 K and 480 cm^2 V^{-1} s^{-1} at 92 K. In the following analysis we will use the mobility values measured at 92 K. Our data are consistent with those reported by other authors [6,7].

8. Electron diffusion

The trigger for cosmic ray events was made up of three scintillators placed two on the top and one at the bottom of the dewar. They are in coincidence with the signals from two groups of 16 horizontal wires each,
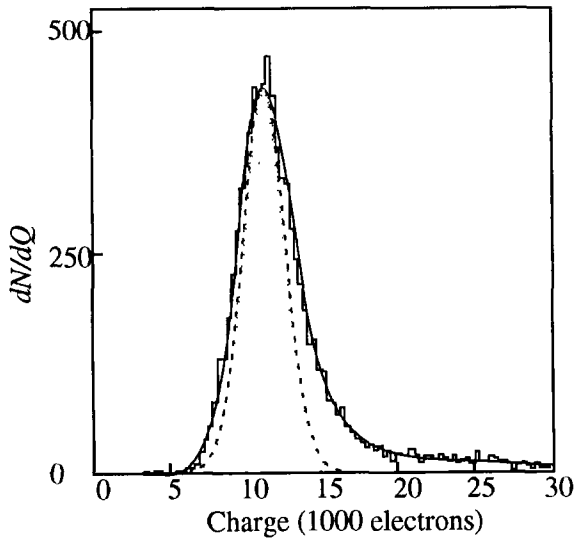
Fig. 14. Collected charge distribution for 2 mm samples of vertical muon tracks. ($E = 500$ V/cm; drift time = 20–40 μs). The continuous curve is the result of the fit described in the text; the shaded area is the Gaussian contribution of the 1400 electrons rms.

one group at the top and one group at the bottom of the wire chamber. The trigger for muons stopping in the detector was the same but without the lowest scintillator and with the lowest group of wires in anti-coincidence. The external trigger provides the $t = 0$ to the system. Events were visually selected requiring the absence of large multiple scattering and of delta rays to obtain a sample of minimum ionising particle (m.i.p.) tracks (barring the relativistic rise). The sample was divided in bins, 20 μs wide, of the measured drift time. For each drift time bin we plotted the distribution of the charge collected on the (horizontal) collection sense wires, proportional to the energy deposited by a m.i.p. in 2 mm length.

Fig. 14 shows, as an example, the distribution for the 20–40 μs bin of drift time at 500 V/cm drift field. The distribution is fitted with the convolution of a Landau distribution and a Gaussian function; the latter (shown as a shaded area in the figure) takes into account of the effects of the electronic noise, the muons spectrum (not all the muons are minimum ionising) and of the effect of the finite electron lifetime. The fit gives, in the example, a peak value of 11 100 electrons and an rms of the Gaussian of 1400 electrons compatible with the above mentioned effects. The intrinsic width of the Landau distribution is much smaller, 500 electrons; this implies that the energy resolution for dE/dx is dominated by the electronic noise.

The sample of minimum ionising tracks crossing vertically the drift volume was used to measure the electron lifetime, as mentioned in section 2, and to

extract a second parameter, the longitudinal diffusion coefficient D. This parameter is important because it can influence the definition of track images and the accuracy of the drift coordinate measurements. Accurate measurements of the diffusion coefficient have been done by Shibamura et al. [8], but they are relative to the transverse coefficient, that in principle can be different from the longitudinal one, and are at fields above 2 kV/cm. We do not know of published measurements at lower fields.

We obtain the longitudinal diffusion coefficient from the analysis of the rise time (R_T) of the signal of the collection wires. The square of the latter is the sum of a constant term ($R_{T_0}^2$) and of a term proportional to the square of the spread (σ^2) of the signal due to diffusion. Also, if t is the drift time and ν the drift velocity, we have $\sigma^2 = 2Dt/\nu^2$. In conclusion a linear fit of R_T^2 (or equivalently σ^2) versus drift time gives directly the longitudinal diffusion coefficient D. We took data at drift field intensities of 350, 250, 150 and 100 V/cm. For each sample we fitted the signal rise shape with the convolution of a step function and of a gaussian. The fitted values of the variance of the Gaussian are shown in Fig. 15. Linear fits to the data give, at the different fields, values that are equal inside the errors. Taking their average we obtain $D = 4.8 \pm 0.2$ cm^2/s.

At the relatively low field intensities of our data, the electrons are expected to be thermal; in this case the Einstein relation $qD/\mu = kT$ should hold. With the mobility value that we have measured, $\mu = 480$ cm^2 V^{-1} s^{-1}, we then expect $D = 3.8$ cm^2/s. A further contribution to the diffusion is known to come from the Coulomb repulsion amongst the electrons. Calculating their contribution with the approximated method of ref. [8] we find a value of about 2 cm^2/s, that should be added (linearly not quadratically). We can conclude that our measured value agrees with the expectations.

9. Free electron yield and recombination

Using again the vertical muons sample we studied systematically the electron-ion recombination at low fields, namely between 100 and 500 V/cm. The vertical muons are, in a first approximation, minimum ionising tracks, parallel to the coordinate planes. The (horizontal) collection wires sample 2 mm long segments of the track. The peak values of the charge distribution at each electric field are presented in Fig. 16: it is, as expected, an increasing function of the field intensity. The asymptotic value at high fields is obtained from the known value of dE/dx through Monte Carlo simulation. We calculate the most probable energy deposition in 2 mm long track to be 326 keV, corresponding to 13 800 electrons (23.6 eV/pair).
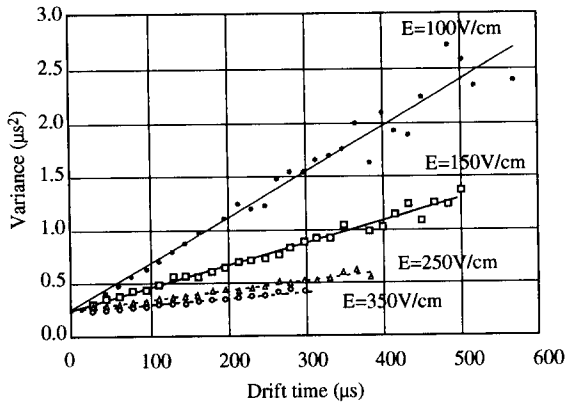
Fig. 15. Pulse rise time squared vs drift time for different fields.

In Fig. 16 we show also the prediction of the On-sager model (arbitrarily) normalised at the highest field (500 V/cm). As expected it disagrees with the data.

An interesting feature of the liquid argon TPC is its ability to measure dE/dx, giving important information for particle identification and for determining the direction of a stopping particle. To study the capability of the detector of identifying particles by dE/dx as a function of the range and the recombination dependence on dE/dx we studied a sample of muons stopping within the chamber, with an identified decay electron. Fig. 17 shows how the ionisation increases when the muons slow down.

At any given point of the muon track the residual range is measured, hence the muon energy is known. The corresponding $\langle dE/dx \rangle$ is obtained, by the Monte Carlo simulation described in section 6. The average value of dQ/dx for that value of the range is extracted from the data sample. The correlation between
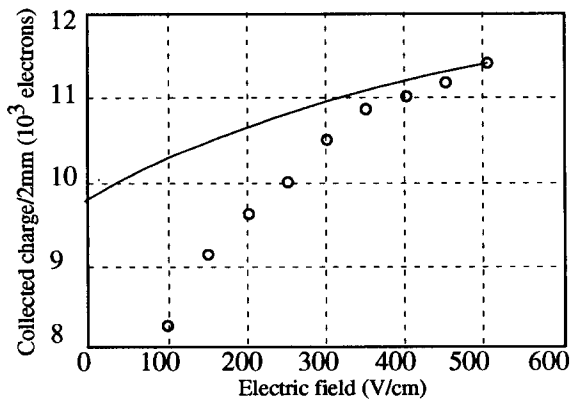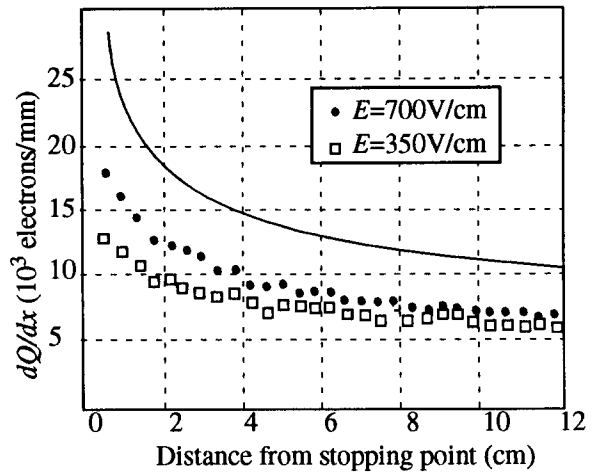

Fig. 17. Average collected charge as a function of the distance from the end point of stopping muons. Curve is the result of a Monte Carlo calculation not including recombination.

$\langle dQ/dx \rangle$ (data) and $\langle dE/dx \rangle$ (Monte Carlo), for three different fields, is shown in Fig. 18. At each field the point at the lowest energy loss is obtained from minimum ionising muon tracks.

As we lack a full theoretical understanding of the recombination process, we fitted the data in Fig. 18 at each field with a phenomenological formula, called the Birks' law:

$$\frac{dQ}{dx} = A \frac{dE/dx}{1 + k_b \frac{dE}{dx}},$$

where A and k_b are constant to be obtained from the fit: the constant A is the asymptotic value of the collected charge per unit length corresponding to a unitary specific energy loss. It is expected to be inde-

Fig. 16. Charge collected on 2 mm length as a function of field for vertical muons. The curve is the Onsager model normalised at 500 V/cm.
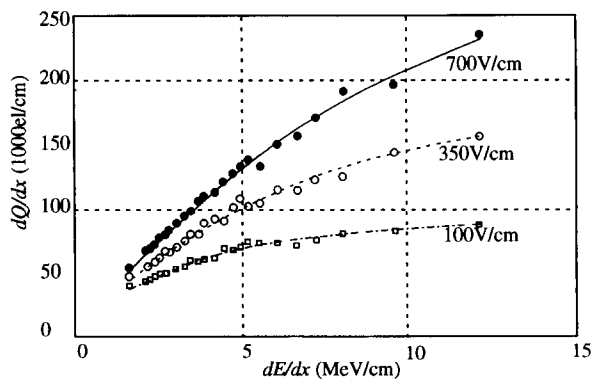

Fig. 18. $\langle dQ/dx \rangle$ as a function of $\langle dE/dx \rangle$ at different fields (stopping muons data). Curves are from fit described in the text.

pendent of field and approximately (given the roughness of the model) equal to 42 electrons/keV. The Birks constant k_b gives the nonlinear dependence: it is expected to be a decreasing function of the field. The curves in Fig. 18 are the results of the fits, that describe well the data. The corresponding values of the constants at 100, 350 and 700 V/cm are respectively: $A = 36 \pm 1$, 33 ± 1 and 36 ± 1 electrons/keV and $k_b = 0.326 \pm 0.019$, 0.130 ± 0.008 and 0.072 ± 0.004 cm/MeV.

The nonlinear dependence of the collected charge on the deposited energy at the low field values, where the liquid argon TPC is operated, affects both the dE/dx measurements and the energy resolution. Due to the recombination process, especially at high specific ionisation values and at low fields, part of the energy deposited by the ionising particle appears not as free charge but as photons, that are not detected. We are considering the possibility of doping the liquid argon to recuperate as free charge part of the energy escaping detection.

10. Space resolution

The space resolution along the drift coordinate has been measured using the tracks from vertical muons at distances from the wire planes such that the maximum drift time is, for each field, less than 250 μs. To avoid the contribution of multiple scattering we evaluate the resolution taking in turn the drift times measured on any three contiguous collection wires; we then take the distance (in time) from the line through the two outer points to the middle one. If d is the corresponding distance along the drift coordinate, the resolution σ is given as a function of its root mean square value by: $\sigma = \sqrt{\frac{2}{3}\langle d^2 \rangle}$. As can be seen in Fig. 19, the resolution is around 150 μm and appears to be independent of the field in our range of intensities.

We expect, on the other hand a dependence on the drift time. The result at $E = 350$ V/cm, again for drift times less than 250 μs, is shown in Fig. 20 (data at different fields show similar behaviour). The curve is the result of a Monte Carlo simulation taking into account the contributions of the noise and of the diffusion.

Different sources contribute to the measured space resolution in the drift direction: 1) the combined effect of electronic noise and diffusion of the electron cloud during drift (rms σ_1), 2) the channel to channel difference in the effective origin of time due to different cables lengths and to different slopes of the output signals (σ_2), 3) out of plane position of the wires (σ_3). The convolution of contributions 1 and 2 (σ_t) has been measured by means of the test pulse, as shown in Figs.
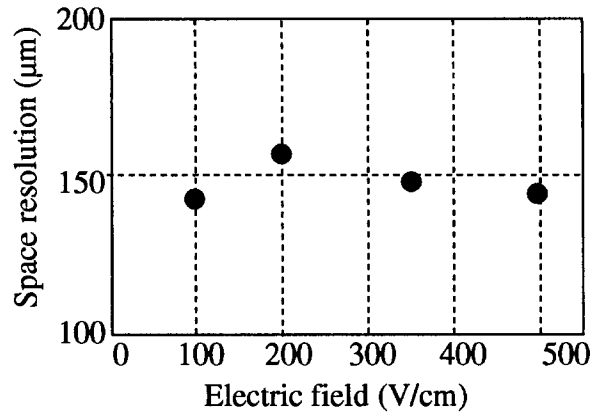

Fig. 19. Space resolution in the drift coordinate vs drift field from vertical tracks within 250μs drift time.

11 and 12. The quantity σ_2 is evaluated by measuring the average time difference for the test pulse in neighbouring channels. It has a small value, $\sigma_2 = 18$ ns. From Fig. 12 we see that, in our operating conditions (S/N = 7–10) this is a small contribution to σ_t, and that it is reached at high values of S/N. The quantity σ_3 is evaluated, using vertical muons, measuring the drift time difference between a channel and the average of the two contiguous ones. The result is $\sigma_3 = 18$ μm, again a small contribution. The remaining contribution to the space resolution comes from the combined effect of longitudinal diffusion and electronic noise. The signal rise time comes from the two causes: the longitudinal charge distribution due to diffusion and the time taken by the electrons to cross the distance (2 mm) between screening and sense planes.

To interpret the data in Fig. 20 note that they are taken at 350 V/cm, where we have a signal to noise
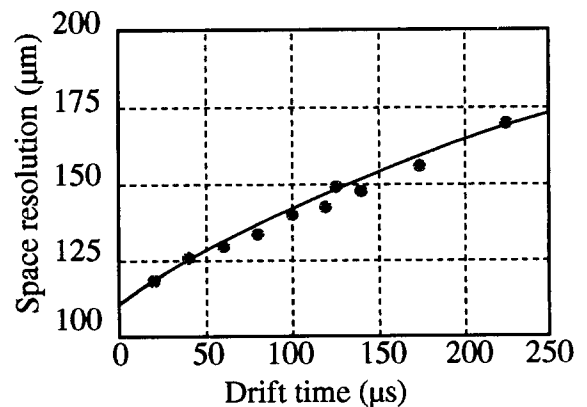

Fig. 20. Resolution in the drift coordinate measured vs drift time (350 V/cm). Curve is from the Monte Carlo simulation described in the text.

ratio $S/N \approx 8$. (We see from Fig. 16 that the signal is 10500 electrons and from the discussion in section 5 the noise is 1300 electrons). The pulse rise time, averaged on the sample, is 1.5 µs. From test pulse data similar to those shown in Figs. 11 and 12 we have for comparison $\sigma_t \approx 120$ ns. The measured drift velocity (see Fig. 13) is $\nu = 1.25$ mm/µs. We can finally calculate this contribution to space resolution as $\nu\sigma_t = 1.25$ µm/ns × 120 ns ≈ 150 µm. In conclusion the calculated value is equal to the measured total resolution as shown in Fig. 20: the combined effect of the rise time and electronic noise determines the space resolution.

As we have noticed the resolution is almost independent of the field intensity. To understand this aspect we recall that the data are relative, for all fields, to tracks at drift times less than 250 µs. As a consequence the average signal rise time is the same for all the samples. At lower fields the signal is smaller, due to increased recombination, and σ_t becomes larger (for example going from 500 to 250 V/cm S/N decreases by 20% and σ_t increases by about 23%). On the other hand the drift velocity decreases (by 25% in the above example) and both effects almost perfectly compensate each other.

The curve shown in Fig. 20 is the prediction of the Monte Carlo simulation and agrees with the data.

11. Energy resolution at a few MeV

The energy resolution for low energy electron tracks can be evaluated by studying the Compton spectrum and the pair production peak produced by a monochromatic gamma ray source placed just outside the dewar. At energies higher than 3 MeV only composite sources are available able to produce monochromatic gamma rays (e.g.: Pu–Ca giving a 6.13 MeV γ or Am–Be emitting a 4.43 MeV γ). Unfortunately these gamma rays are always accompanied by neutrons whose interaction rate is equal or higher to that of the gammas. As the energy spectrum of the neutrons extends from thermal energies to about 8–10 MeV, their interaction products with the argon nuclei (nuclear capture or inelastic collisions with subsequent emission of gamma and beta rays) could result in a non-negligible background not easily removable. We have chosen to use an Am–Be source that emits monochromatic gamma rays of 4.43 MeV. Its n–γ ratio is about one. The source is placed outside the dewar, close to its lateral wall 1 m below the top flange and it is collimated by means of lead blocks in such a way that the Compton and pairs electrons are produced as close as possible to the wire chamber. As the radiation length in liquid Ar is 14 cm, nearly all the γs entering the active volume of the detector (45 cm in radius) should produce a visible ionising event.

The source emits 2×10^3 γ/s as well as 2.5×10^3 n/s over 4π. The presence of neutrons increases the background due to the natural radioactivity. In fact, due to inelastic and capture reactions both on argon and stainless steel, the neutrons produce γ rays with a wide energy spectrum. The total background can be measured by shielding completely the source with 20 cm of lead which absorbs all the γ emitted directly by the source and leaves the neutron spectrum practically unchanged. In this test it is crucial to exploit the self-triggering capabilities of our device. Our recent measurements demonstrated that we can trigger on isolated events with energy down to ≈ 1 MeV simply using the integrated signal coming from the collection wires. We collected data with the threshold at 1.8 MeV. With this threshold and using 16 wires the trigger rates are the following: without source 5.1 Hz, with shielded source 5.6 Hz, with unshielded source 8.5 Hz.

In practice, to reduce the event size hence to maximise the acquisition rate, the analogue signals from the collection wires are grouped sixteen by sixteen and are used independently to trigger the acquisition and to localise the chamber wires hit by the ionising event. Only a small volume around the triggering track (16 wires times 51 µs ≈ 4 kbyte) is stored on tape. The cosmic ray events are rejected with good efficiency simply requiring that only one group of sixteen wires has a signal above threshold.

We have collected data at a drift field of 500 V/cm and analysed them using the algorithms described in section 4. Fig. 21 shows as an example the collection view of two electrons of 7.5 and 2 MeV respectively.

The Compton scattering theory predicts a slowly increasing energy distribution of the scattered electron with a sharp falling edge corresponding to the 4.20 MeV ($\approx E\gamma - 2m_e/E\gamma$, $E\gamma$ = incoming γ energy); the pair production peak should appear as a narrow line centred at 3.41 MeV ($E\gamma - 2m_e$). The pair production probability versus Compton scattering is at this energy about 30%. In the experimental data this value is somehow reduced because the γs having Compton-scattered once can subsequently reinteract producing
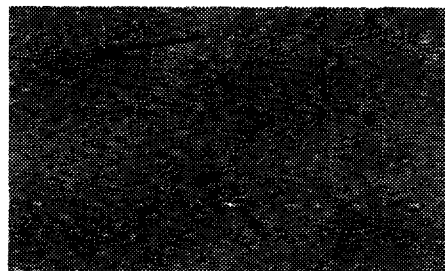

Fig. 21. Collected view of 7.5 and of a 2 MeV electrons. The drift coordinate corresponds to the horizontal axis.
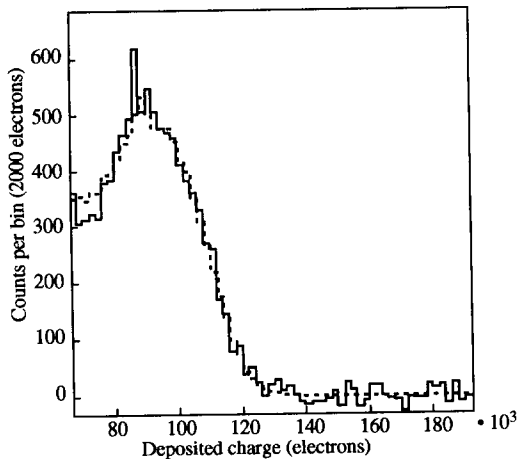
Fig. 22. Compton spectrum (background subtracted). The dotted curve shows the Monte Carlo calculation described in the text.

other electrons which in turn can trigger the data acquisition. The ratio between the position of the Compton edge and the pair peak is a check that we are really dealing with the interaction products of the 4.43 MeV γ source; the smearing of the edge and the peak in the experimental distribution is directly related to the detector energy resolution.

Fig. 22 shows the background subtracted energy spectrum; it corresponds to about 45 000 triggers with the unshielded source and 28 000 with shielded source (background). The Compton edge and the pair peak are clearly visible. To interpret the data we have generated 100 000 events with the Monte Carlo program described in section 6; the simulation takes into account all the interactions of the photons and electrons in the detector; its geometry is completely described in the program. The deposited energy is transformed into detected charge taking into account the loss due to the finite electron lifetime, taken to be 2.5 ms (the data cannot be corrected for this effect, because we do not have a $t = 0$ signal, hence we do not know the distance of the event from the wire plane). The free electron yield is adjusted to 66% to fit the data. The detected charge is then smeared with a Gaussian shape with $\sigma_Q/Q = 7\%$ also adjusted to fit the data. The Monte Carlo reproduces well the data. We conclude that, after subtracting the electron lifetime contribution, the energy resolution for electrons around 4 MeV is $\sigma_E/E = 7\%$. The main contributions to the energy resolution for an electron of ≈ 4 MeV are:

1) The effective electronic noise contribution, including that of the off-line extraction of the signal which is ≈ 1300 electrons, as we discussed in section 5, while the average number of wire hit is 6; this gives a contribution to the energy measurement error of 3.8%.

2) Uncertainty on the charge amplifiers calibration constants (2%).

3) Missing parts of the track: since the signal extraction algorithm has a threshold at about 6000 electrons (in order to reject efficiently the noise), we miss part of the deposited charge especially at the start and end of the track; this translates into a rms of ≈ 3500 electrons corresponding to 3.5%.

The best results obtained in liquid argon are those of Aprile et al. [10]. They measured the energy resolution for the 976 keV internal conversion electrons from ^{207}Bi at different field values, finding a noise subtracted resolution of $\pm 4.7\%$ at 500 V/cm. In order to compare the two results we must subtract from our resolution the contribution, due not only to the electronic noise, but also to points 2) and 3), absent in the measurement of Aprile et al. Subtracting in quadrature we are left with $\sigma_E/E = 4.3\%$ in good agreement with those authors. As we have mentioned 66% of the ion pairs produced by electrons of a few MeV at a field of 500 V/cm, do not recombine. This value can be compared with the measurement of Aprile et al. [10] at 1 MeV and a field of 500 V/cm, that found 67% and with the 60% obtained by Scalettar et al. [9] using 364 keV electrons, i.e. at a lower energy. As discussed in section 8, we have measured the free electron yield also for minimum ionising particles; we find that the fraction of free ionisation charge at 500 V/cm is 83%. These differences could be interpreted as consequences of the nonlinear dependence of the free charge on the deposited energy at high values of dE/dx, because at lower energy the ionisation increases rapidly near the end point of the track.

12. Conclusions

We have performed the analysis of the data taken with a three-ton liquid argon TPC, that we operated smoothly and without interruptions for more than two years at CERN. The detector is providing bubble chamber grade three-dimensional pictures of events induced by cosmic rays and radioactive sources. We have systematically investigated the performance and the physical parameters of the detector analysing these events. The physical parameters (electron drift velocity, electron lifetime, free electron yield, electron diffusion coefficient) have been found to be consistent with the expectation, confirming the design detector performance. The space resolution in the drift coordinate, found to be of the order of 100 μm, and the superior particle identification capability are powerful tools for the detailed study of rare underground events as foreseen by the ICARUS experiment. The energy resolution in the MeV region, as determined from the data from radioactive sources, is of a few percent, as ex-

pected and as needed for the solar neutrino program of ICARUS.

The in-depth understanding of the basic physics aspects of the liquid argon TPC allows us to conclude that such a detector can be built in large sizes. The basic assumptions we made in the original proposal of the ICARUS experiment have been experimentally verified. The experience gained in operating a medium size prototype has shown that a multi-kiloton detector can be reliably operated over long periods of time.

Acknowledgements

References

[1] ICARUS collaboration, ICARUS a proposal for the Gran Sasso Laboratory, INFN/AE-85/7 Frascati (1985).
[2] P. Benetti et al., Nucl. Instr. and Meth. A 332 (1993) 395.
[3] A. Bettini et al., Nucl. Instr. and Meth. A 305 (1991) 177.
[4] O. Buneman, T.E. Cranshaw, and J.A. Harvey, Can. J. Res., A 27 (1949) 191.
[5] GEANT version 3.1516.
[6] L.S. Miller, S. Howe and W.E. Spear, Phys. Rev. 166 (1968) 871.
[7] W.F. Schmidt, IEEE Trans. Electr. Ins. EI-19 (1984) 389.
[8] E. Shibamura, T. Takahashi, S. Kubota and T. Doke, Phys. Rev. A 20 (1979) 2547.
[9] R.T. Scalettar, P.J. Doe, H.J. Mahler and H.H. Chen, Phys. Rev. A 25 (1982) 2419.
[10] E. Aprile, W.H. Ku and J. Park, IEEE Trans. Nucl. Sci. NS-35 (1988) 37.